Applied Physics B (2023) 129:42
https://doi.org/10.1007/s00340-023-07980-6

**Applied Physics B**
**Lasers and Optics**

RESEARCH

# Experimental X-ray emission doses from GHz repetitive burst laser irradiation at 100 kHz repetition rate

**Vytenis Barkauskas[1] · Lukas Rimkus[2,3] · Jonas Reklaitis[1] · Artūras Plukis[1] · Mikas Vengris[2,3]**

Received: 1 August 2022 / Accepted: 19 January 2023 / Published online: 16 February 2023


## Abstract

Material processing with high repetition rate ultra-short laser pulses with intensities higher than $10^{13}$ W/cm$^2$ may lead to the X-ray emission dose exceeding allowed dose limits. We have investigated a worse-case exposure scenario, in which laser processing parameters were tuned to maximize X-ray yield. Use of double pulse regime leads to increase of the X-ray yield up to two orders of magnitude compared with the single pulse regime. $H'(0.07)$ and $H^*(10)$ dose rates were measured using X-ray spectrometer and electronic dosimeter. Maximum dose rates at 35 cm distance from the X-ray source calculated using spectrometer data exceeded 1 Sv/h and 9 mSv/h, respectively. Dose rates measured using the dosimeter were lower. The difference is attributed to narrower X-ray spectral range detectable by dosimeters, which may lead to underestimation of exposure doses in the laser processing laboratories. The presented method might be used as an example to evaluate X-ray yield and optimize measures of radiation protection.

## 1 Introduction

Recent development of ultra-short pulse lasers allows to achieve very high power irradiation (in PW scale) and high pulse repetition rate (in GHz scale). The applications of such lasers in industry varies from material processing to medical applications [1–4]. Although focused beams allows to achieve $10^{22}$ W/cm$^2$, or even higher intensities [5], the requirements of most everyday applications are much lower. Table-top high repetition rate lasers usually achieve moderate intensities up to $10^{17}$ W/cm$^2$. Nevertheless, an inevitable consequence of irradiating matter with such light intensities is the generation of X-ray.

The efficient and potentially hazardous (when exposure of radiation exceeds dose limits set in safety requirements. This may have negative consequences for human health.) X-ray generation becomes possible at the intensities of $10^{13}$ W/cm$^2$ [6]. When femtosecond laser pulse of such intensity interacts with the material, the electrons are torn off from the atoms and quasi-neutral plasma is created. The electrons of the plasma are further accelerated by the electric field of the laser light and decelerated by the deflections or collisions with the other particles of the matter. Deceleration results in bremsstrahlung continuum radiation. At electron energies high enough to kick out the electrons from the inner shells of target atoms, characteristic X-ray fluorescence lines are emitted when inner shell holes are filled by the recombination electrons. The energy of produced X-ray photons is directly related to the electron temperature ($T_e$) of plasma, which is a function of laser intensity ($I_L$)and wavelength ($\lambda_L$) and could be written as $T_e \sim I_L \lambda_L^2$ [7]. Typically, peak intensities between $10^{13}$–$10^{15}$ W/cm$^2$ result in X-ray energies ranging from a few keV to several tens of keV. [8–10]. This effect allows to create the source of ultrashort X-ray pulses, however in other applications, e.g. laser processing, the negative effect of hazardous ionizing radiation generation is observed. This problem has been recently addressed in the works by different authors [11–15].

Until recently, it was generally thought that the intensity range of $10^{13}$–$10^{14}$ W/cm$^2$ was not enough to cause serious radiation hazard concerns [6]. However, recent studies have shown that not to be the case, especially when the small pre-pulses are introduced before the main pulse [16–18]. The smaller intensity pre-pulse creates pre-plasma which increases driving pulse coupling and X-ray generation

✉ Vytenis Barkauskas
vytenis.barkauskas@gmail.com

1 Department of Nuclear Research, Center for Physical Sciences and Technology, Savanoriu Ave. 231, Vilnius 02300, Lithuania

2 Laser Research Centre, Vilnius University, Saulėtekio Ave. 10, Vilnius 10223, Lithuania

3 Light Conversion, Keramiku st. 2B, Vilnius 10233, Lithuania

efficiency [19, 20]. The overall efficiency highly depends on the delay and intensity of the pre-pulse. Particularly, if tunable GHz and MHz bursts produced by the lasers with burst-in-burst feature [21] are used during material processing, the leading pulses within the burst can also create pre-plasma and X-ray emission might increase drastically [22]. When materials are processed in ambient air or in shielding gas, the intensity of laser field is clamped at a certain value due to the photoionization and self-induced defocusing [23]. This effect limits the maximum achievable intensity and possible doses in such applications. The air strongly absorbs ionizing radiation with photon energies up to about 5 keV [12] and this reduces the X-ray dose level at greater distances. When lasers with high average power and high repetition rates are used, the dose can accumulate over time, therefore repetition rate should also be considered in radiological hazard analysis. Survey meters and dosimeters may be used for dose measurements during laser material processing [14]. Data acquired from X-ray spectral measurements may also be used for dose calculations using experimental parameters and relevant dose factors [24].

ICRP recommended effective dose limits in planned exposure situations are 20 mSv/y for occupational exposures averaged over a period of 5 year and 1 mSv/y for the members of the public. Such doses are typically measured using ambient dose equivalent $H^*(10)$, representing a deep radiation dose at a depth of 10 mm below the skin. The $H'(0.07)$ equivalent dose measurements are used for shallow dose measurements, representing a shallow dose at a depth of 0.07 mm below the skin. ICRP recommendations for annual equivalent dose in the skin ($H'(0.07)$) are 500 mSv/y for occupational exposures and 50 mSv/y for public members [25]. The studies in this field show that this limit might be easily exceeded during laser operation [14], therefore analysis of radiological hazards in the laser micromachining laboratories should be performed. In this paper, we present experimental investigation of doses resulting from X-ray generation during laser processing. We have attempted to simulate a worst-case exposure scenario by tweaking the process parameters to maximize X-ray yield, then measure maximum X-ray doses evaluating potential hazard and effective shielding.

## 2 Experimental setup

The experiment using femtosecond laser pulses was performed in order to measure dose rates and cumulative doses. An amplified solid-state laser Carbide from Light Conversion [21] featuring laser radiation with a maximum average power of 90 W, a repetition frequency of 0.1–2 MHz, with a central wavelength of 1030 nm and a variable pulse duration (0.24–10 ps) was used. The laser was configured to produce the bursts of pulses. In the burst mode, the laser output pulse train consists of pulse packets instead of single pulses. Each packet consists of a certain number of equally separated pulses. MHz-Burst contains pulses with a nanosecond period (~ 13.15 ns), GHz-Burst contains pulses with a picosecond period (~ 440 ps) [21].

The laser radiation was focused using $f = +150$ mm spherical lens into a spinning metal target, which was translated during the measurements to have a fresh target spot for every shot. A focused beam spot size diameter was ~ 25 µm (FWHM). The laser pulse energy was changed in the range of 100–900 µJ which corresponds to $6.5\times10^{13}$ – $5\times10^{14}$ W/cm$^2$ intensity. In different experiments, when the pulse energy or other parameters were changed the focusing distance was also optimized to obtain the maximum X-ray yield. The target was based on a rotating disk geometry, which was continuously translated along the radial direction in the focal plane, and the laser pulse angle of incidence was kept at zero. The disk rotation speed was ~ 800 RPM, corresponding to the linear velocity of 4.2 m/s at the inner radius (5 cm) and the 8.4 m/s at the outer radius of the target (10 cm). In contrast, the lowest calculated speed required for each consecutive laser pulse separation was ~ 4.5 m/s at 100 kHz.

Direct measurements of the X-ray emission spectra from plasma with an energy resolution of 140 eV and 50 eV channel width were done using an Amptek X-123SDD spectrometer in the single-photon counting regime which uses a thermoelectrically cooled Si-PIN junction detector (area—25 mm$^2$, thickness—0.5 mm) with 21.5 mm$^2$ collimator before it. This type of spectrometers are commonly used to measure the spectral photon flux in pulsed radiation fields. Before entering detector, the incident photons passed a protective 25 µm Be foil and the collimator.

To attenuate X-ray signal, different thinness Al foil filters of varying thickness were placed before the spectrometer. These filters allowed to attenuate X-ray flux under ~ 6 keV, minimizing the spectrometer total count input rate below 10 % of applied laser pulse repetition rate and avoiding possible detector saturation and photon pile-up phenomena [26]. The distance between the spectrometer and the target was also changed during the experimental session. When X-ray source was optimized and the final X-ray fluence measured the distance between focal spot and spectrometer was 220 cm, with ~ 10° angle to the target plane and 21 µm Al foil in front of detector (see Fig. 1). To calculate the energy-dependent fluence, the transmission of the filters, position of the spectrometer, and the detector efficiency were taken into account.

It is important to stress out that X-ray dose might vary on the detection angle [6], however in our calculations, we assumed the angular distribution of X-rays from the laser-driven plasma sources to be almost isotropic [27, 28].

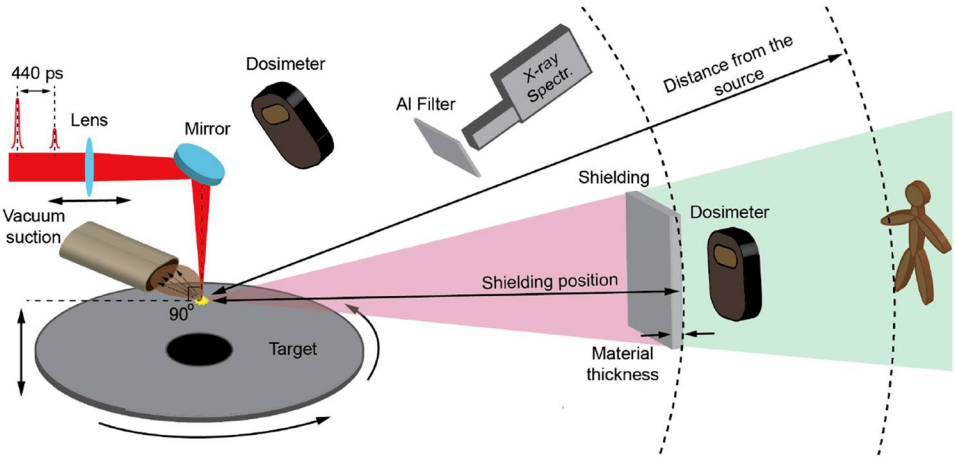


**Fig. 1** The experimental setup

X-ray doses were measured using electronic and thermoluminescence dosimeters. Electronic semiconductor dosimeter (Thermoscientific EPD-N2) was used for dose rate measurements. This personal-type dosimeter detects photons within an energy range of 20 keV to 10 MeV and was placed 35 cm away from the laser focal spot. Thermoluminescence dosimeters were used to monitor integral doses at the different spots in the laboratory during whole experimental session. Thermoluminescence dosimeters were capable to measure doses from 0.01 mSv to 10 Sv, in the energy range from 10 keV to 10 MeV.

## 3 Results

The experiment of X-ray generation optimization and irradiation doses measurement was performed to evaluate potential ionizing radiation hazard. It is important to mention that even 20 influencing factors might be counted, affecting X-ray photon emissions arising from ultrashort pulse laser materials processing [16]. All parameters that, according to our knowledge, could have the highest impact on X-ray yield and also were possible to tune were optimized to obtain the maximum X-ray yield. The recently published paper explains the detailed X-ray yield optimization experiments of such X-ray source [29]. A number of different MHz and GHz laser burst configurations, focusing conditions, amplitude ratio between the prepulse and the driving pulse, delay time of prepulse, disk rotation speed and other parameters were investigated in the mentioned paper. Moreover, it was observed that vacuum suction near the plasma spot increases registered X-ray signal (presumably, by limiting reabsorption and scattering losses due to debris).

It is important to stress that in this work, we only investigate the highest X-ray emission scenario when maximal dose values are registered, and these parameters were found to give highest X-ray yield: GHz-Burst with two pulses, total energy of 0.9 mJ in both pulses and the energy ratio 1/10 between the pulses (second pulse was 10 times greater than the first one). Repetition rate was 100 kHz, pulse duration was minimal (240 fs) and the average laser power was maximal (90 W). The target spinning and translation speed, debris vacuum suction near the plasma were also optimized. The X-ray spectra at maximum X-ray yield for different materials used during experiments are shown in Fig. 2.

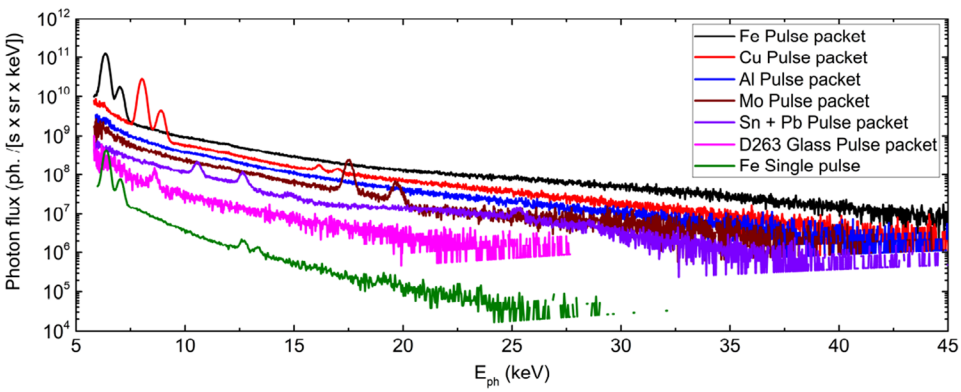


**Fig. 2** Calculated spectral photon flux for different target materials at 100 kHz repetition rate. The driving pulse energy without prepulse is $E_{DR} = 0.9$ mJ, the driving pulse energy with prepulse is $E_{DR} = 0.82$ mJ, and the prepulse energy is $E_{PP} = 0.08$ mJ

The upper energy limit of photons generated in the targets using mentioned parameters reached 45 keV. This value is close to the detection limit set for this experiment. Thus even higher energy photons might be expected. Maximum photon energy of 45 keV corresponds well with the spectral modeling results using electron temperature scaling, which predicts highest electron temperature [9, 10]. Measurements using single pulse regime were also performed. Single pulse regime results in much smaller (more than 200 times) intensity than use of double-pulse. The reason for this difference is that smaller intensity pre-pulse creates pre-plasma which increases driving pulse coupling and X-ray generation efficiency [19, 20, 30]. Since we tried to maximize X-ray yield by optimizing earlier mentioned parameters (especially amplitude ratio between prepulse and driving pulse), we see a more than 200 times increase in X-ray yield compared with 30 times increase that was reported earlier by using a similar laser system [22], where the envelope of the pulse train is adjusted to ensure that each pulse in the burst has an identical pulse energy. It is important to add that it has been shown that introducing lower intensity prepulse before the main pulse can increase the soft X-ray yield up to 100 times compared with the single pulse operation [30].

By knowing irradiated detector area, spectrometer distance from the X-ray source (220 cm), air and aluminum transmission spectrum, measurement time (60 s) and using dose conversion coefficients [31] the $H'(0.07)$ and $H^*(10)$ spectral dose rates (SPD) were calculated at 35 cm distance from the X-ray source. The dose rates were calculated using Eq. 1:

$$\mathrm{SPD}(E_n) = \frac{\frac{\mathrm{Ph}(E_n)}{\mathrm{Eff}(E_n)\times D} \times \frac{1}{T_{\mathrm{Al}}(E_n,d)} \times \frac{1}{T_{\mathrm{Air}}(E_n,R-r)} \times \mathrm{DCC}(E_n)}{t} \times \frac{R^2}{r^2}, \quad (1)$$

where $D$—irradiated area of Si-PIN detector, $\mathrm{Ph}(E_n)$—number of detected photons at a certain energy channel, $\mathrm{Eff}(E_n)$—energy dependent spectrometer efficiency, $T_{Al}(\mathrm{E}_n, \mathrm{d})$, $T_{\mathrm{Air}}(E_n, \mathrm{R\text{-}r})$—energy and thickness dependent values of Al, air transmission, $d$—thickness of Al filter before spectrometer, $R$—distance between spectrometer and Fe target, $r$—distance from the X-ray source where the dose rates are evaluated, $\mathrm{DCC}(E_n)$—energy dependent dose conversion coefficients, $t$—measurement time.

When the spectral dose rate is known the dose rate could be simply calculated using:

$$\text{Dose rate} = \sum_n \mathrm{SPD}(E_n). \quad (2)$$

The calculated spectral dose rates for Fe are given in Fig. 3. The comparison of $H'(0.07)$ and $H^*(10)$ show that highest contribution for the skin dose ($H'(0.07)$) comes from the low energy photons (up to approx. 20 keV), while the contribution for $H^*(10)$ starts to grow at higher energies.

The calculated dose rates using spectral data for different target materials are given in Table 1. The highest integral dose rate in 6–45 keV range at 35 cm distance from source measured using spectrometer was $H^*(10) = 8.94$ mSv/h and $H'(0.07) = 1276$ mSv/h. These dose rates were achieved using iron target. The dose rates that were measured with electronic dosimeter at 35 cm distance from the X-ray source was $H^*(10) = 3.1$ mSv/h and $H'(0.07) = 5.2$ mSv/h.

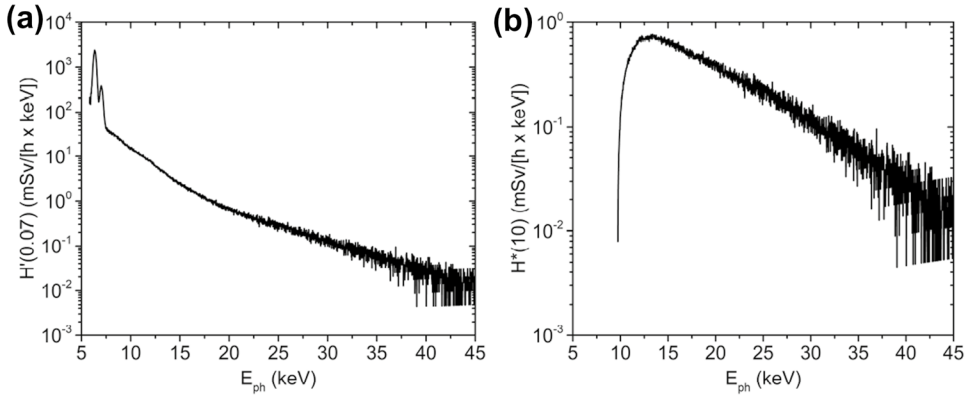


**Fig. 3** Iron (Fe) X-ray spectral dose rate **a** $H'(0.07)$ and **b** $H^*(10)$ at 35 cm from the X-ray source

**Table 1** $H^*(10)$ and $H'(0.07)$ dose rates for different target materials calculated using spectral data (in mSv/h)

| | Fe | Cu | Al | Mo | D263 Glass | Sn + Pb |
|---|---|---|---|---|---|---|
| $H^*(10)$ | 8.94 | 4.73 | 2.95 | 1.18 | 0.13 | 0.77 |
| $H'(0.07)$ | 1276 | 448 | 107 | 62 | 9.95 | 33.6 |

Measurements performed at 100 kHz repetition rate, the driving pulse energy with prepulse is $E_{\mathrm{DR}} = 0.82$ mJ, and the prepulse energy is $E_{\mathrm{PP}} = 0.08$ mJ

Compared to the calculated values using spectral measurements the dose rates measured using the dosimeter were about three times lower for $H^*(10)$ and about 250 times lower for $H'(0.07)$. One reason for this might be the dead time of the detector [32, 33]. However, the main reason for this difference could be attributed to the fact that the dosimeter used had designed detection energy limit of 20 keV and all photons below this level were omitted as expected.

The low energy limit for such dosimeters has no significant impact in their common applications measuring doses from gamma or neutron sources due to a fact that gamma and neutrons usually have much (one or two orders of magnitude) higher energies. In this experiment the use of such dosimeters was motivated by the fact that there are no commercial dosimeters which allow measuring doses at very low (below 10–20 keV) energies. This suggests that when dosimeters are used to measure doses caused by bremsstrahlung irradiation at low energies (5–45 keV) the dose values obtained underestimates the exposure doses. We demonstrate this experimentally and we conclude that application of standard dosimeters to estimate doses in the laser lab is not straightforward. Doses measured by such dosimeters should be analyzed only taking into account the spectral properties of the ionizing radiation. X-ray spectrometer can detect individual photons and measure the energy spectra, which is particularly important if adequate radiation protection shielding is to be calculated. The energy dependent fluence measured using spectrometer can be translated to exposure dose using dose factors. It is important to add that ionization-chamber based survey meters have been used in most measurements of the X-ray radiation field emitted in laser material processing [6, 14]. As we see from the spectra above, the largest part of ionizing radiation energy occurs in the low energy region, which is not covered by conventional dosimeters. Another problem with the usual personal dosimeters is that they were designed and tested with continuous X-ray sources and their response in pulsed fields (especially with ultrashort pulses) is still a matter of investigation [33–36] and is outside the scope of this paper.

The targets of other metals besides Fe were investigated as well. The obtained dose rates measured for Cu and Al targets using dosimeters were, respectively, 2 and 3 times lower for $H^*(10)$ and 3 and 12 times lower for $H'(0.07)$ in comparison with Fe targets. However targets of heavier elements (Mo, Sn, Pb) showed one order of magnitude lower dose rates for $H^*(10)$: 0.66 mSv/h (Mo), 0.22 mSv/h (Sn + Pb), 0.16 mSv/h (Pb). This contradicts the results obtained using modelling [10], which predicted increasing doses with increasing target atomic number. It is known that bremsstrahlung intensity scales with square of the atomic number [37]. The results obtained in modelling [10] were in an agreement with this fact. Therefore we expected some increment in X-ray emission with $Z$ in the experimental measurements, however our experimental data using double pulse regime does not follow this trend. Atomic number of Mo ($Z = 42$) is higher than Fe ($Z = 26$) or Cu ($Z = 29$), but X-ray emission is almost one order of magnitude lower. We believe that other factors like melting point, laser light reflection and absorption, may have considerable impact for generated X-ray intensity [38]. It may be the material for an additional study outside of the discussion of this paper.

Data presented in Table 1 show that dose rates during such experiments are high and dose limits for personnel operating in such environments may be easily exceeded. Therefore precautionary measures should be taken. Usually the combination of three main different measures are taken: (1) minimization of the exposure time, (2) maximization of the distance from the X-ray source, (3) effective shielding utilization. The first principle is ensured by applying cumulative dose limits, which are set in the requirements for the occupational exposure. The time limit can be calculated knowing dose limit and dose rate during irradiation.

In case of $H^*(10)$ dose rate of 9 mSv/h and ($H'(0.07)$) dose rate of 1276 mSv/h, allowed non-occupational doses (1 mSv/year and 50 mSv/year, respectively), would be exceeded in several minutes. It would take a bit longer to exceed allowed occupational doses (20 mSv/year and 500 mSv/year respectively), however the conclusion is that additional protective measures should be taken, as time limitation would eliminate personnel from working in the lab.

For the second principle, the air attenuation and dose quadratic dependence from the distance should be accounted. Finally, for the third principle the different materials attenuation should be known and their thicknesses could be evaluated.

In Fig. 4 it is shown how the dose value depends on the distance from the X-ray source in air. From this evaluation

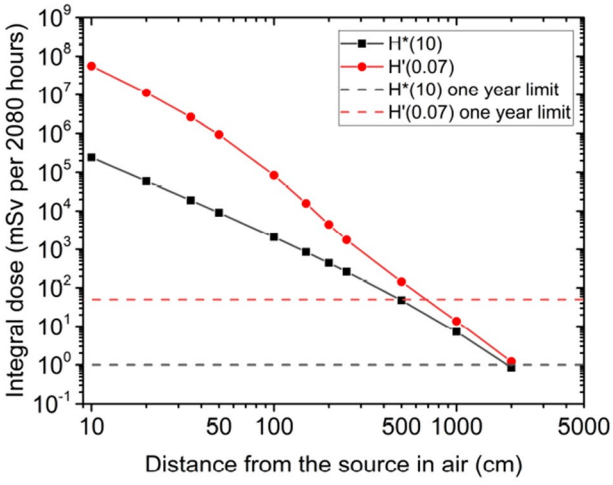


**Fig. 4** Calculated $H^*(10)$ and $H'(0.07)$ dose dependence on distance from the X-ray source in air per 2080 h

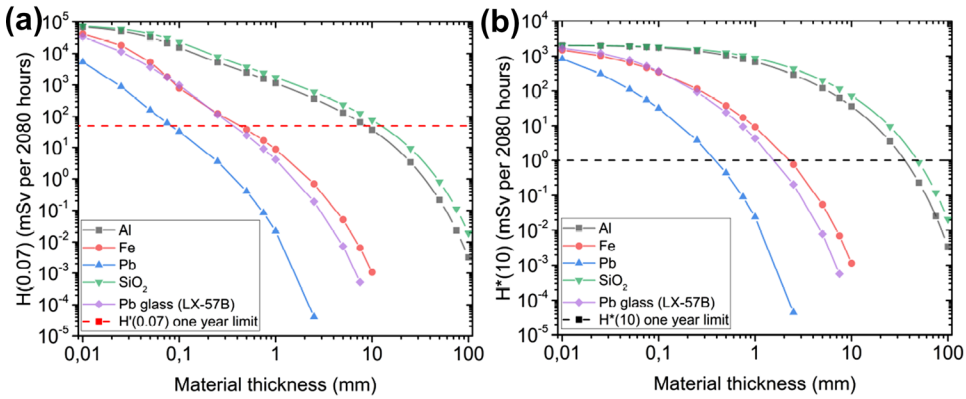


**Fig. 5** Calculated **a** $H'(0.07)$ and **b** $H^*(10)$ dose dependence on shielding material thickness at 100 cm distance from X-ray source per 2080 h

it is seen that safe distance from unshielded source for $H'(0.07)$ is around 7 m and for $H^*(10)$ is around 20 m.

Dose dependency on the shielding material thickness at 100 cm distance from the X-ray source was evaluated. The results are shown in Fig. 5. For the $H^*(10)$ dose to be lower than recommended dose, the safe lead thickness should be more than 0.4 mm, LX-57B glass thickness should be more than 1.6 mm, iron thickness should be more than 2.3 mm, aluminum thickness should be more than 35.7 mm and $SiO_2$ thickness should be more than 48.3 mm.

During experimental session passive thermoluminescence dosimeters were used to evaluate cumulative dose levels. The specified lower energy limit of this dosimeter was 10 keV. Experiments were performed for 3 weeks (15 days in the lab). This should not be treated as continuous optimal operation of the equipment: the adjustment of the setup was performed constantly, with laser turned off, therefore it is very difficult to evaluate the real time of the irradiation. However, this does represent the typical irradiation schedule of a laser research laboratory; in production environment, where laser micromachining stations are operational 24/7, the presented results would underestimate the doses by one or more orders of magnitude. We report these results as a complementary monitoring data which we obtained during experimental session. The dosimeter closest to the target (31 cm away) measured $H^*(10)$ dose of 32.4 mSv and $H'(0.07)$ dose of 2.05 Sv during experimental session. Another dosimeter which was behind 3 mm thick iron plate, with the same distance from the target measured 0.04 mSv and 0.33 mSv above background respectively. Personal-type dosimeter, which was placed at lab worker working place (~ 2 m from the X-ray source), showed only 0.01 mSv above the background. This implies that the chosen thickness of 3 mm iron shielding was sufficient to attenuate the dose below recommended limits.

Finally the possible cumulative doses were calculated using highest registered dose conditions at 35 cm away from the target. In 2080 h (typical work year) the integral $H^*(10)$ dose at this distance would be 18.95 Sv and the integral $H'(0.07)$ dose would be 2633 Sv without any shielding or protection, which is more than 4 orders higher than recommended dose for public users. Such possible doses indicate that precautionary measures should be taken to avoid irradiation above the set limits.

## 4 Summary and conclusions

The experimental investigation of doses resulting from X-ray generation during femtosecond laser processing was performed. The laser, beam delivery and target parameters affecting X-ray generation efficiency were optimized to maximize X-ray yield. The use of double-pulse regime resulted in up to 200 times higher X-ray intensity in comparison with the single pulse regime. Maximum X-ray dose rates were measured to be $H^*(10) = 8.94$ mSv/h and $H'(0.07) = 1276$ mSv/h for the iron target. At such dose rates the doses accumulated within typical work year 35 cm away from the target would exceed recommended irradiation dose more than 4 orders of magnitude. Therefore simple precautionary measures were investigated to limit the irradiation doses. The most practical measure to protect workers from ionizing radiation emerging from femtosecond laser material processing was identified to be shielding using metal plates. It was also found that dose measurements using electronic dosimeters may be evaluated incorrectly due to electronic dosimeter energy limits. The presented methods might be used as an example to evaluate X-ray yield in laser processing facilities and optimize measures of radiation protection.

**Acknowledgements** This project has received funding from European Social Fund (project No 09.3.3-LMT-K-712-19-0014) under grant agreement with the Research Council of Lithuania (LMTLT).

**Author contributions** V.B.: Conceptualization, Methodology, Validation, Investigation, Resources, Writing original draft, Funding acquisition, L.R: Conceptualization, Methodology, Validation, Formal Analysis, Investigation, Resources, Writing - Original Draft, Visualization, J.R.: Investigation, Resources, A.P.: Supervision, Funding acquisition,

M.V.: Conceptualization, Methodology, Software, Validation, Writing - Review & Editing, Supervision, Project administration.

**Data availability** The datasets generated during and/or analysed during the current study are available from the corresponding author on reasonable request.

## Declarations

**Conflict of interest** The authors declare no competing interests.

## References


1. K. Sugioka, Progress in ultrafast laser processing and future prospects. Nanophotonics **6**(2), 393–413 (2017). https://doi.org/10.1515/nanoph-2016-0004
2. F. Morin, F. Druon, M. Hanna, P. Georges, Microjoule femtosecond fiber laser at 1.6 $\mu$m for corneal surgery applications. Opt. Lett. **34**(13), 1991–1993 (2009). https://doi.org/10.1364/OL.34.001991
3. M. Malinauskas, A. Žukauskas, S. Hasegawa, Y. Hayasaki, V. Mizeikis, R. Buividas, S. Juodkazis, Ultrafast laser processing of materials: from science to industry. Light Sci. Appl. **5**(8), 16133 (2016). https://doi.org/10.1038/lsa.2016.133
4. S.A. Ashforth, R.N. Oosterbeek, O.L.C. Bodley, C. Mohr, C. Aguergaray, M.C. Simpson, Femtosecond lasers for high-precision orthopedic surgery. Lasers Med. Sci. **35**(6), 1263–1270 (2020). https://doi.org/10.1007/s10103-019-02899-x
5. S. Weber, S. Bechet, S. Borneis, L. Brabec, M. Bučka, E. Chacon-Golcher, M. Ciappina, M. DeMarco, A. Fajstavr, K. Falk, E.R. Garcia, J. Grosz, Y.J. Gu, J.C. Hernandez, M. Holec, P. Janečka, M. Jantač, M. Jirka, H. Kadlecova, D. Khikhlukha, O. Klimo, G. Korn, D. Kramer, D. Kumar, T. Lastovička, P. Lutoslawski, L. Morejon, V. Olšovcová, M. Rajdl, O. Renner, B. Rus, S. Singh, M. Šmid, M. Sokol, R. Versaci, R. Vrána, M. Vranic, J. Vyskočil, A. Wolf, Q. Yu, P3: an installation for high-energy density plasma physics and ultra-high intensity laser-matter interaction at ELI-beamlines. Matter Radiat. Extremes **2**(4), 149–176 (2017). https://doi.org/10.1016/j.mre.2017.03.003
6. H. Legall, C. Schwanke, S. Pentzien, G. Dittmar, J. Bonse, J. Krüger, X-ray emission as a potential hazard during ultrashort pulse laser material processing. Appl. Phys. A **124**(6), 407 (2018). https://doi.org/10.1007/s00339-018-1828-6
7. W. Kruer, *The Physics of Laser Plasma Interactions* (Addison-Wesley, Boston, 1988)
8. P. Gibbon, Efficient production of fast electrons from femtosecond laser interaction with solid targets. Phys. Rev. Lett. **73**(5), 664–667 (1994). https://doi.org/10.1103/PhysRevLett.73.664
9. F.N. Beg, A.R. Bell, A.E. Dangor, C.N. Danson, A.P. Fews, M.E. Glinsky, B.A. Hammel, P. Lee, P.A. Norreys, M. Tatarakis, A study of picosecond laser-solid interactions up to $10^{19}$ W/cm$^2$. Phys. Plasmas **4**(2), 447–457 (1997). https://doi.org/10.1063/1.872103
10. V. Barkauskas, A. Plukis, Prediction of the irradiation doses from ultrashort laser-solid interactions using different temperature scalings at moderate laser intensities. J. Radiol. Prot. **42**(1), 011501 (2022). https://doi.org/10.1088/1361-6498/ac44fb
11. M.J. Wesolowski, C.C. Scott, B. Wales, A. Ramadhan, S. Al-Tuairqi, S.N. Wanasundara, K.S. Karim, J.H. Sanderson, C.A. Wesolowski, P.S. Babyn, X-ray dosimetry during low-intensity femtosecond laser ablation of molybdenum in ambient conditions. IEEE Trans. Nucl. Sci. **64**(9), 2519–2522 (2017)
12. R. Weber, R. Giedl-Wagner, D.J. Förster, A. Pauli, T. Graf, J.E. Balmer, Expected X-ray dose rates resulting from industrial ultrafast laser applications. Appl. Phys. A **125**(9), 635 (2019)
13. J. Reklaitis, V. Barkauskas, A. Plukis, V. Kovalevskij, M. Gaspariūnas, D. Germanas, J. Garankin, T. Stanislauskas, K. Jasiūnas, V. Remeikis, Emission and dose characterization of the 1 kHz repetition rate high-Z metal K$\alpha$ source driven by 20 mJ femtosecond pulses. Appl. Phys. B **125**(3), 41 (2019)
14. H. Legall, J. Bonse, J. Krüger, Review of X-ray exposure and safety issues arising from ultra-short pulse laser material processing. J. Radiol. Prot. **41**(1), 28–42 (2021). https://doi.org/10.1088/1361-6498/abcb16
15. L. Martín, J. Benlliure, D. Cortina-Gil, J. Peñas, C. Ruiz, Improved stability of a compact vacuum-free laser-plasma X-ray source. High Power Laser Sci. Eng. **8**, 18 (2020). https://doi.org/10.1017/hpl.2020.15
16. J. Schille, S. Kraft, T. Pflug, C. Scholz, M. Clair, A. Horn, U. Loeschner, Study on X-ray emission using ultrashort pulsed lasers in materials processing. Materials **14**(16) (2021). https://doi.org/10.3390/ma14164537
17. J. Schille, S. Kraft, D. Kattan, U. Löschner, Enhanced X-ray emissions arising from high pulse repetition frequency ultrashort pulse laser materials processing. Materials **15**(8) (2022). https://doi.org/10.3390/ma15082748
18. J. Holland, R. Weber, M. Sailer, C. Hagenlocher, T. Graf, Pulse duration dependency of the X-ray emission during materials processing with ultrashort laser pulses. Procedia CIRP **111**, 855–858 (2022)
19. W. Lu, M. Nicoul, U. Shymanovich, A. Tarasevitch, P. Zhou, K. Sokolowski-Tinten, D.v.d. Linde, M. Masek, P. Gibbon, U. Teubner, Optimized Kalpha X-ray flashes from femtosecond-laser-irradiated foils. Phys. Rev. E Stat. Nonlinear Soft Matter Phys. **80**(2) (2009). https://doi.org/10.1103/PHYSREVE.80.026404
20. M. Afshari, P. Krumey, D. Menn, M. Nicoul, F. Brinks, A. Tarasevitch, K. Sokolowski-Tinten, Time-resolved diffraction with an optimized short pulse laser plasma X-ray source. Struct. Dyn. **7**(1), 014301 (2020). https://doi.org/10.1063/1.5126316
21. M. Barkauskas, K. Neimontas, V. Butkus. Device and method for generation of high repetition rate laser pulse bursts. Google Patents (2020)
22. D. Metzner, M. Olbrich, P. Lickschat, A. Horn, S. Weissmantel, X-ray generation by laser ablation using MHz to GHz pulse bursts. J. Laser Appl. **33**(3), 032014 (2021). https://doi.org/10.2351/7.0000403
23. A.A. Garmatina, B.G. Bravy, F.V. Potemkin, M.M. Nazarov, V.M. Gordienko, Intensity clamping and controlled efficiency of X-ray generation under femtosecond laser interaction with nanostructured target in air and helium. J. Phys. Conf. Ser. **1692**(1), 012004 (2020). https://doi.org/10.1088/1742-6596/1692/1/012004
24. Conversion Coefficients for use in Radiological Protection against External Radiation. ICRP Publication 74. Ann. ICRP **26**(3-4) (1996)
25. The 2007 Recommendations of the International Commission on Radiological Protection. ICRP publication 103. Ann. ICRP **37**(2-4), 1–332 (2007). https://doi.org/10.1016/j.icrp.2007.10.003
26. W. Becker, *Advanced Time-Correlated Single Photon Counting Techniques* (Springer, Berlin, 2005), pp.263–346. https://doi.org/10.1007/3-540-28882-1_7
27. Y. Hironaka, K.G. Nakamura, K. Kondo, Angular distribution of X-ray emission from a copper target irradiated with a femtosecond laser. Appl. Phys. Lett. **77**(25), 4110–4111 (2000). https://doi.org/10.1063/1.1335841
28. B. Hou, A. Mordovanakis, J. Easter, K. Krushelnick, J.A. Nees, Directional properties of hard X-ray sources generated by tightly

focused ultrafast laser pulses. Appl. Phys. Lett. **93**(20), 201503 (2008). https://doi.org/10.1063/1.3023065
29. L. Rimkus, I. Stasevičius, M. Barkauskas, L. Giniūnas, V. Barkauskas, S. Butkus, M. Vengris, Compact high-flux X-ray source based on irradiation of solid targets by gigahertz and megahertz bursts of femtosecond laser pulses. Opt. Contin. **1**(8), 1819–1836 (2022). https://doi.org/10.1364/OPTCON.463291
30. H. Nakano, T. Nishikawa, H. Ahn, N. Uesugi, Temporal evolution of soft X-ray pulse emitted from aluminum plasma produced by a pair of Ti:sapphire laser pulses. Appl. Phys. Lett. **69**(20), 2992–2994 (1996). https://doi.org/10.1063/1.117754
31. N. Petoussi-Henss, W. Bolch, K. Eckerman, A. Endo, N. Hertel, J. Hunt, M. Pelliccioni, H. Schlattl, M. Zankl, Conversion coefficients for radiological protection quantities for external radiation exposures. Ann. ICRP **40**(2–5), 1–257 (2010). https://doi.org/10.1016/j.icrp.2011.10.001
32. P. Ambrosi, M. Borowski, M. Iwatschenko, Considerations concerning the use of counting active personal dosemeters in pulsed fields of ionising radiation. Radiat. Prot. Dosim. **139**(4), 483–493 (2010). https://doi.org/10.1093/rpd/ncp286
33. U. Ankerhold, O. Hupe, P. Ambrosi, Deficiencies of active electronic radiation protection dosemeters in pulsed fields. Radiat. Prot. Dosim. **135**(3), 149–153 (2009). https://doi.org/10.1093/rpd/ncp099
34. O. Hupe, H. Zutz, J. Klammer, Radiation protection dosimetry in pulsed radiation fields. IRPA 13 Glasgow (2012)
35. M. Gotz, Dosimetry of highly pulsed radiation fields. PhD thesis, Technischen Universität Dresden (2018). https://www.hzdr.de/publications/PublDoc-12055.pdf
36. K. Makarevich, R. Beyer, J. Henniger, Y. Ma, S. Polter, M. Sommer, T. Teichmann, D. Weinberger, T. Kormoll, Active dosimetry with the ability to distinguish pulsed and non-pulsed dose rate contributions. EPJ Web Conf. **253**, 09001 (2021). https://doi.org/10.1051/epjconf/202125309001
37. E. Haug, W. Nakel, *The Elementary Process of Bremsstrahlung* (World Scientific, Singapore, 2004). https://doi.org/10.1142/5371
38. A. Krygier, G.E. Kemp, F. Coppari, D.B. Thorn, D. Bradley, A. Do, J.H. Eggert, W. Hsing, S.F. Khan, C. Krauland, O.L. Landen, M.J. MacDonald, J.M. McNaney, H.S. Park, B.A. Remington, M. Rubery, M.B. Schneider, H. Sio, Y. Ping, Optimized continuum X-ray emission from laser-generated plasma. Appl. Phys. Lett. **117**(25), 251106 (2020). https://doi.org/10.1063/5.0033629